Graphene at fluidic interfaces

Belyaeva, L.A.

APPENDIX 1

Supporting Information to Chapter 2

1.1. Methods

1.1.1. Growth and transferring of graphene

Copper foil with the thickness of 25 μm was annealed at 1035°C and the monolayer graphene films were grown using chemical vapor deposition.[1] After the chemical vapor deposition (CVD) synthesis, the graphene grown on the backside of the copper foil was removed by using oxygen plasma. After etching the graphene at the backside of the copper foil, the piece was placed at the interface of a biphasic mixture of cyclohexane and water supplemented with ammonium persulfate (*i.e.* the copper etchant). For transferring the graphene onto substrates with the interfacial caging method the approaches described in the "Results" section of Chapter 2 were followed. All samples were rinsed with water and ethanol after the transfer. For the poly(methyl methacrylate) (PMMA)-assisted method the protocol from Reference 2 was reproduced. For the contact stamping method a wafer was directly placed on graphene floating on the etchant, transferred and rinsed with water; alternatively, the etchant is replaced by pure water prior stamping. For the hexane-assisted transfer method reproduced the protocol from Reference 3 was reproduced: placed a wafer beneath graphene (in the etchant) and fishing from below the graphene with hexane as the top phase. In all four transfer methods 0.5 M solution of $(NH_4)_2S_2O_8$ was used as copper etchant.

1.1.2. Characterization

Raman spectroscopy

Micro-Raman spectroscopy was performed with a commercial inVia model from Renishaw spectrometer set-up with a dual-axis XY piezo stage. A laser with 532 nm excitation wavelength was used. The grating has 600 lines/mm. Raman spectra are recorded in air with a 100x objective. The laser power was limited to below 2 mW to prevent any laser induced heating of the samples.

Atomic force microscopy (AFM)

All AFM experiments with graphene on silicon wafers were carried out on Multimode Bruker (ex-DI) Nanoscope V. The experiments were performed using a silicon 254 probe (AC160TS, Asylum Research) with 300 kHz nominal resonance

frequency. The images were scanned in an intermittent contact mode at room temperature with 512×512 pixels. All the samples have been annealed at 400^{o}C prior to the imaging.

Scanning electron microscopy (SEM)

SEM of graphene transferred to TEM quantifoil grids was performed with a FEI NANOSEM 200 at 10 kV. For the measurements graphene samples were transferred to quantifoil grids using the interfacial caging method.

1.1.3. Electrical measurements

To evaluate the quality of the transferred graphene in a large area, in this study graphene transistors with a channel length of several millimeters were fabricated. As the contact resistance between our graphene and metal electrodes (both are of large area) is negligible, a two-point source-drain measurements were applied and all the results were normalized by using the length/width ratio of the graphene transistors to obtain the field-effect mobility values.The transistor characteristics of the electrolyte-gated graphene field-effect transistor devices with different geometry were tested using a home-made setup. For that, a SR830 DSP lock-in amplifier with narrow filters was used to recover weak signal from a noisy background. The electrolyte gate voltage V_{ref} (up to ±0.4 V) was applied to a Ag/AgCl reference electrode immersed in the electrolyte. For the electrical probing of graphene samples floating at the biphasic interface, the etchant solution was replaced with 0.1 M solution of KCl. During the replacement of the etchant solution, the entire mixture was cooled down to freeze the cyclohexane phase in order to avoid the effect of vibrations on the integrity of the graphene sheet.

1.2. References

1. Pierson, H. O. *Handbook of chemical vapor deposition (CVD)*. (Noyes Publications / William Andrew Publishing, LLC, 1999).

2. Suk, J. W. *et al.* Transfer of CVD-grown monolayer graphene onto arbitrary substrates. *ACS Nano* **5,** 6916–6924 (2011).

3. Zhang, G. *et al.* Versatile polymer-free graphene transfer method and applications. *ACS Appl. Mater. Interfaces* **8,** 8008–8016 (2016).

APPENDIX 2

Supporting Information to Chapter 3

2.1. Methods

2.1.1. Sample preparation

Graphene on copper. All graphene samples were grown on a copper foil by chemical vapor deposition (CVD) method, according to the protocol described in ref[1].

Graphene on Si/SiO_2 wafers and free-standing graphene. CVD graphene grown on copper was transferred to Si/SiO_2 wafers and quantifoil grids using the interfacial caging method.[2]

Graphene at water/air and deuterated water/air interfaces. CVD graphene grown on copper was first placed in a 0.1 M solution of ammonium persulfate (APS) in water for copper etching. After copper removal the solution underneath graphene was replaced with ultrapure water. Slightly wider variations of G and 2D peaks positions were found for graphene floating on an APS solution than for graphene on ultrapure water (see Figure A2.8 of this Appendix), attributing to doping effect, and, therefore, always thoroughly replaced APS with ultrapure water. Although, CVD graphene can stably float on the surface of water, for Raman measurements, it is also advisable to immobilize graphene from moving on the surface. This can be achieved in different ways: by placing a physical limitation, such as a plastic frame around graphene or by using very small volumes of water. The immobilization of graphene does not affect Raman results.

Graphene at a water/cyclohexane and water/1-octanol interfaces. Graphene on copper was first placed on a surface of a 0.1M solution of ammonium persulfate in water. Then cyclohexane (or 1-octanol) was added on top to form a biphasic system with graphene floating at the interface. During etching of the copper, the samples were covered with lids to prevent evaporation of the top organic phase; more cyclohexane (or 1-octanol) was added during experiments to prevent full evaporation of the top phase. After copper removal the bottom phase underneath graphene was replaced with ultrapure water. To minimize graphene movability on the surface of liquids, the size of graphene sample was fitted to the size of the Petri dish.

Hydrogenated graphene-on-copper. Graphene on copper was hydrogenated using a H_2 plasma in a computer controlled Diener plasma generator (1mbar, 10W) for 10 and 60 seconds.[3]

Hydrogenated graphene-on-water. The samples of hydrogenated graphene on copper were placed in a 0.1 M solution of APS for copper etching. After copper was etched away, the solution underneath hydrogenated graphene was replaced with ultrapure water.

2.1.2. Raman spectroscopy

Raman measurements were carried out with confocal spectrometer WITEC at a power below 2mW to avoid excessive thermal damage of graphene, and at excitation wavelengths of 457 nm and 532 nm. 100× objective was used for graphene on copper, graphene on Si/SiO_2 and free-standing graphene; a 70× immersion objective was used for graphene on liquid supports. Graphene/Cu samples were typically cut into 5 mm×10 mm or 10 mm×10 mm pieces, which were then studied by Raman spectroscopy directly on copper. Then graphene was transferred from copper to a SiO_2/Si substrate or a transmission electron microscopy (TEM) grid (for free-standing configuration) using the interfacial caging method,[2] or to liquid interfaces using the method described above. A comparative analysis showed no statistical difference between the samples of 5 mm×10 mm and 10 mm×10 mm (Figure A2.9 of this Appendix). For each substrate or liquid support 3-10 samples were tested, and for each sample 10-20 Raman spectra from different areas of graphene were recorded. There was no significant sample-to-sample variation for all substrates except free-standing graphene (see Figure A2.3 of this Appendix), which is in agreement with other reported studies.[4,5] Noteworthy, because Raman measurements of graphene at liquid interfaces, especially in between two liquids, are technically more challenging, the spectra of such samples are typically more noisy which may have resulted in a less accurate determination and, consequently, the apparent broadening of the 2D width.

Figure A2.1a and b show the intensities of the G and 2D bands of graphene upon scanning across the water/graphene/1-octanol interface, with the position of

highest intensities (blue circles in Figure A2.1a and blue spectrum in Figure A2.1b) corresponding to the separation between the top and the bottom phase. Scanning the same interface without graphene (i.e. the same vertical coordinate and different horizontal positions) and profiling intensities of the solvents, however, do not yield any information about the position of the interface (i.e. there is no difference between the solvents peaks in the bulk phases and near the interface, see Figure A2.2).

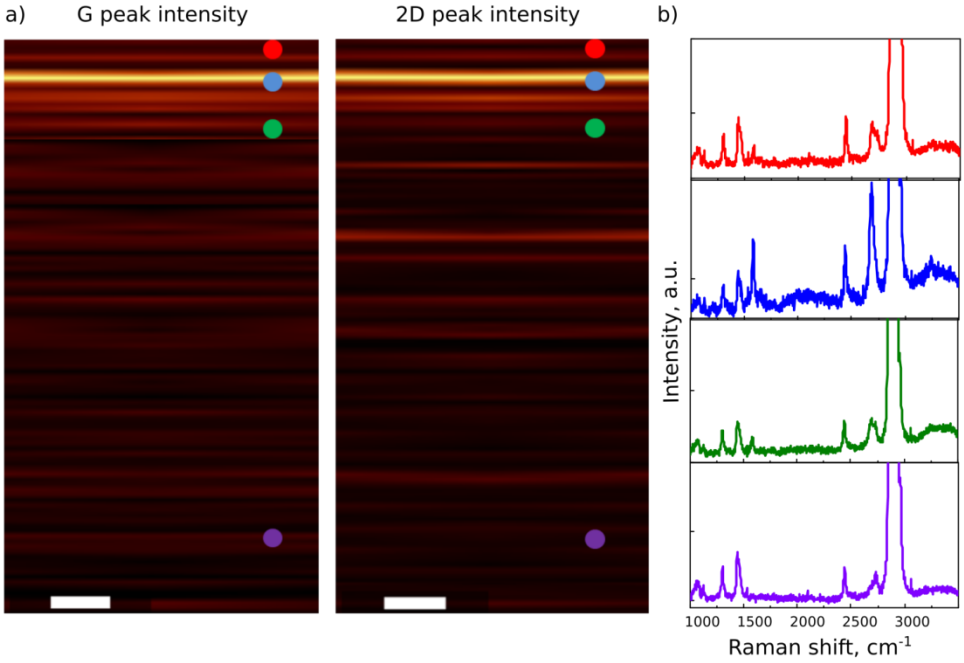

Figure A2.1. In-depth profile Raman scan of graphene at water/1-octanol interface with a 532 nm excitation wavelength. a) In-depth profiles of G and 2D peaks intensities. Coloured circles represent different positions of the measurement area with the respect to the interface between water and 1-octanol (i.e. to the line of maximum intensities of G and 2D peaks): above the interface in the 1-octanol phase (red), at the interface (blue), below but in the vicinity of the interface in the water phase (green), below the interface deeply in the water phase (purple). The scale bars represent 2 μm b) Corresponding Raman spectra recorded above the interface in the 1-octanol phase (red), at the interface (blue), below but in the vicinity of the interface in the water phase (green), below the interface deeply in the water phase (purple).

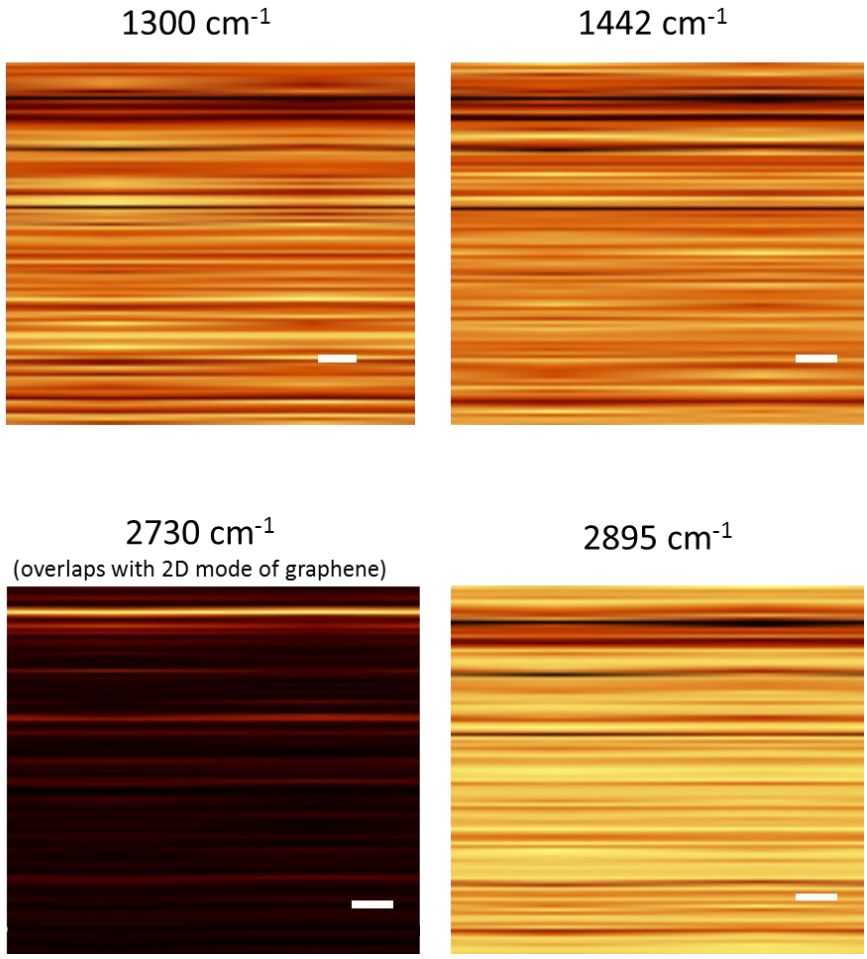

Figure A2.2. An in-depth Raman scan of water/1-octanol interface at 532 nm excitation wavelength. In-depth profiles of the intensities of 1-octanol bands at 1300cm^{-1}, 1442cm^{-1}, 2730cm^{-1} and 2895cm^{-1}. The scale bars represent 2 µm

Table A2.1. Raman bands of biphasically caged graphene, pure water, 1-octanol and cyclohexane at 457 nm and 532 nm excitation wavelengths.

	ω, cm^{-1} (457 nm)	ω, cm^{-1} (532 nm)
graphene (in biphasic caging)	~1585	~1585
	~2730	~2696
water	1640	1640
	2800-3700	2800-3700
1-octanol	1300	1300
	1442	1442
	2730	2730
	2895	2895
cyclohexane	1264	1264
	1442	1442
	2662	2662
	2851	2851
	2922	2922
	2936	2936

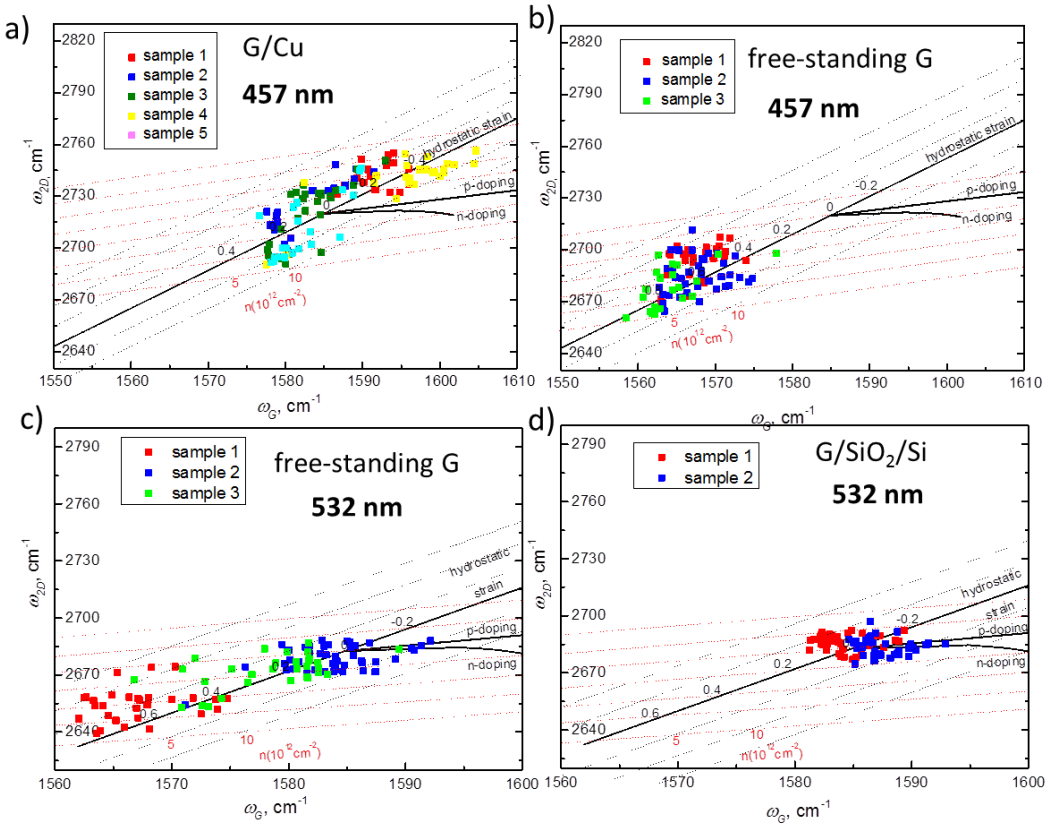

Figure A2.3. Sample to sample variation of the correlation maps of G and 2D peak positions of graphene on different substrates. a) Correlation map of graphene on copper, excitation wavelength 457 nm. b) Correlation map of free-standing graphene, excitation wavelength 457 nm. c) Correlation map of free-standing graphene, excitation wavelength 532 nm. d) correlation map of graphene on Si/SiO_2, excitation wavelength 532 nm.

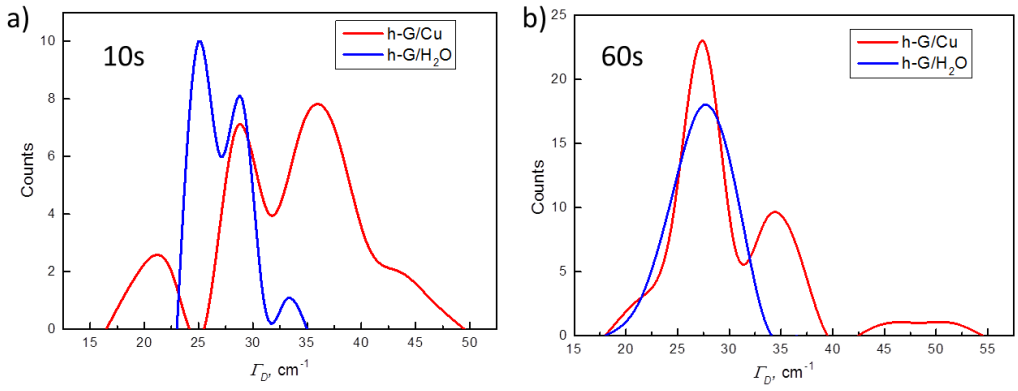

Figure A2.4. Statistical distributions of D peak widths (Γ_D) of hG on copper and water. a) Hydrogenation time 10 s. b) Hydrogenation time 60 s.

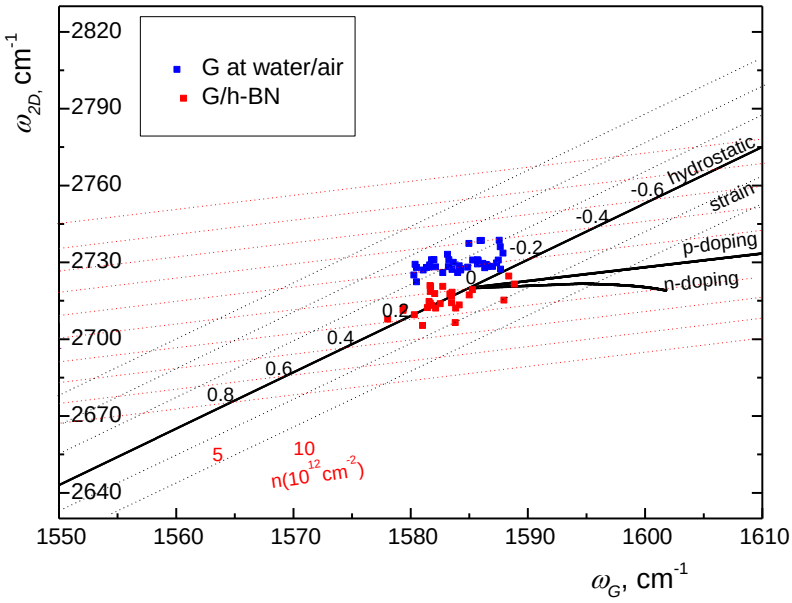

Figure A2.5. Correlation maps of graphene on water and graphene transferred to h-BN/copper, excitation wavelength 457 nm.

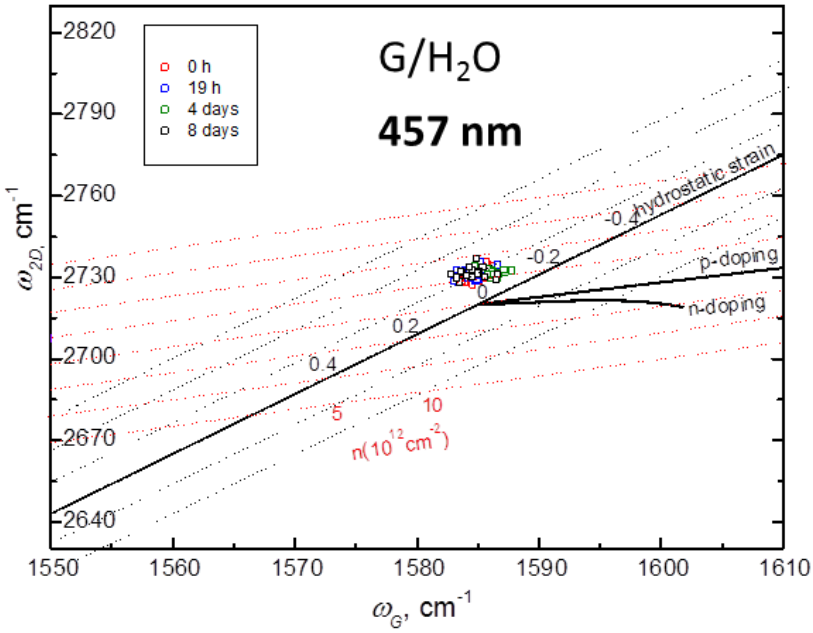

Figure A2.6. Durability of strain relaxation effect of water on graphene. Correlation map of G and 2D Raman frequencies (w_G and w_{2D}) of graphene on water that was floating on the surface of water for 0 hours, 19 hours, 4 days and 8 days.

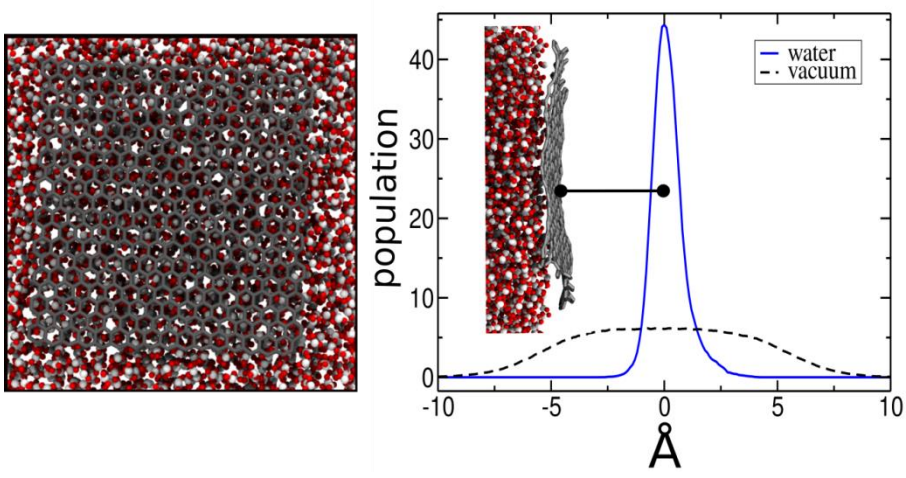

Figure A2.7. MD simulations of graphene on water surface versus graphene in vacuum.

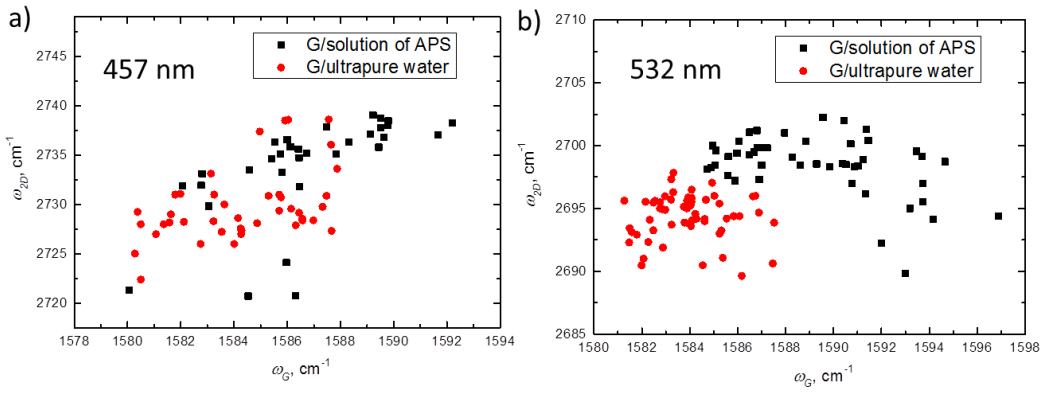

Figure A2.8. Correlation maps of G and 2D peaks frequencies of graphene in APS solution and ultrapure water. a) measured at the excitation wavelength of 457 nm. b) measured at the excitation wavelength of 532 nm.

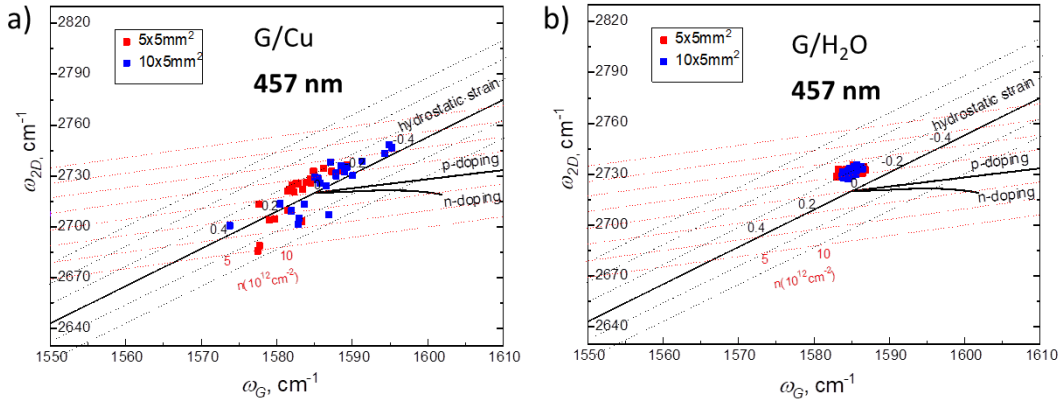

Figure A2.9. Effect of size on the strain and doping distribution in graphene. a) Correlation maps of G and 2D peaks frequencies of graphene/Cu samples in sizes 5 mm×10 mm and 10 mm×10 mm. b) Correlation maps of G and 2D peaks frequencies of graphene/water samples in sizes 5 mm×10 mm and 10 mm×10 mm.

References

1. Fu, W. *et al.* Graphene transistors are insensitive to pH changes in solution. *Nano Lett.* **11,** 3597–3600 (2011).

2. Belyaeva, L. A., Fu, W., Arjmandi-Tash, H. & Schneider, G. F. Molecular caging of graphene with cyclohexane: transfer and electrical transport. *ACS Cent. Sci.* **2,** 904–909 (2016).

3. Jiang, L., Fu, W., Birdja, Y. Y., Koper, M. T. M. & Schneider, G. F. Quantum and electrochemical interplays in hydrogenated graphene. *Nat. Commun.* **9,** 793 (2018).

4. Metten, D., Federspiel, F., Romeo, M. & Berciaud, S. Probing built-in strain in freestanding graphene monolayers by raman spectroscopy. *Phys. Status Solidi Basic Res.* **250,** 2681–2686 (2013).

5. Bendiab, N. *et al.* Unravelling external perturbation effects on the optical phonon response of graphene. *J. Raman Spectrosc.* **49,** 130–145 (2018).

APPENDIX 3

Supporting Information to Chapter 4

3.1. Methods

3.1.1. Materials

Two types of graphene were used: monolayer graphene on a copper substrate provided by Graphenea and graphene grown in a tube oven on a 25 μm copper foil at 1035° according to the procedure described in ref.[1]. Before conducting contact angle experiments the backside of graphene-on-copper (G/Cu) was removed with O_2 plasma. Both types of graphene show the same results for water contact angle measurements. Multilayered graphene was prepared by repetitive PMMA transfer[2] of graphene on G/Cu.[3,4] Highly Oriented Pyrolytic Graphite (***HOPG,*** 7x7x0.8-1.8 mm with mosaic spread 0.8-1.2 degree) was purchased from NT-MDT.

3.1.2. Sample preparation

CVD graphene on a copper substrate was placed in a 0.3 M water solution of ammonium persulfate (APS) (98% Sigma-Aldrich). Once the copper foil was etched away the APS solution was repeatedly replaced with ultrapure water by sequential diluting steps yielding a clean graphene surface without any observable APS crystals.[1] In general, presence of ions in water has very small effect on the surface tension of water – in the order of 3% or lower at the concentration of 0.3 M[5–7] – and, therefore, negligible effects on the measured contact angle. Consequently, and given the precautions undertaken to replace the etching APS solution by water, possible presence of residual ions had no effect on the contact angle measurements (the CA of graphene in 0.1 M $FeCl_3$ is equal to the CA of graphene in pure water, Figure A3.1 of this Appendix).

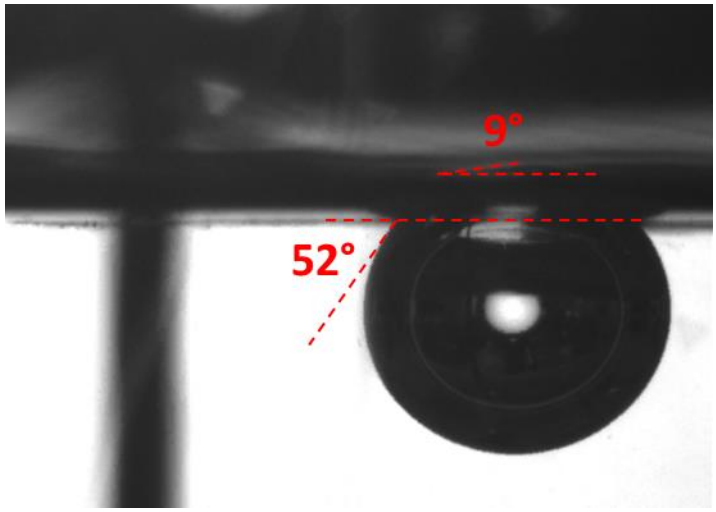

Figure A3.1. Contact angle of graphene on the surface of a 0.1 M aqueous solution of $FeCl_3$. Presence of ions in concentrations below 0.3 M does not affect the measured contact angle, the contact angles of graphene in different etchant solutions are equal to the contact angle of graphene in pure water.

To place a 6 µl air bubble under the water-graphene-air interface, air was injected through a J-shaped inverted needle underneath the graphene (Figure 4.2a in Chapter 4). The contact angle was then measured at least five times at the three-phase line interface (Figure 4.2d in Chapter 4).

To improve the stability of graphene on the water surface, graphene was surrounded with a Langmuir–Blodgett film of 1,2-dipalmitoyl-*sn*-glycero-3-phosphocholine (DPPC) lipids (Avanti Polar Lipids Inc.) at a surface pressure of 30 mN m^{-1} as it is described in ref.[8,9]. The lipids had a concentration of 1 mg mL^{-1} and were first dissolved in $CHCl_3/CH_3OH$ 3:1 vol %. First, graphene on copper[1] (copper facing down) was placed floating on the etchant solution and the appropriate amount of lipids (depending on the size of the graphene and of the cuvette) was added on the surface of the etchant solution around graphene. The etchant solution was then sequentially replaced with ultrapure water and the contact angle was measured. The lipids are known to only spread on the surface of water

(around the graphene) without adsorbing on its surface (as measured by infra-red spectroscopy).[8,9]

Graphene surrounded with lipids showed a higher stability during the deposition of the air bubble. Both graphene samples, without and with lipids, showed similar measured contact angles, *i.e.* 42°±3° and 42°±3° respectively (Figure A3.2 of this Appendix), confirming the absence of lipids on the graphene surface.

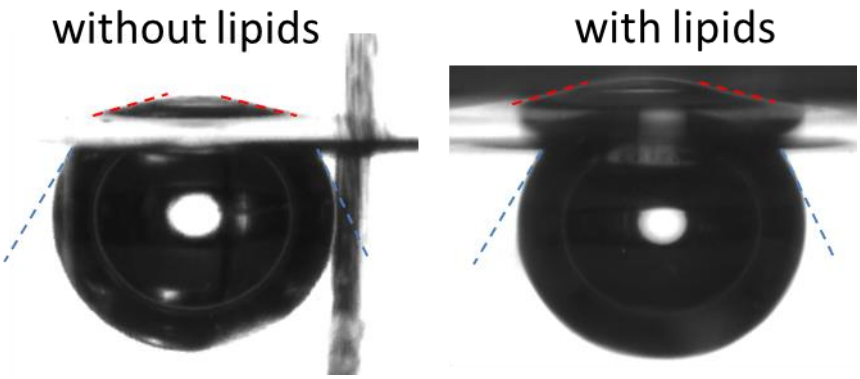

Figure A3.2. Captive bubble on graphene with (right) and without (left) a DPPC (1,2-dipalmitoyl-*sn*-glycero-3-phosphocholine) lipid scaffold. Lipids do not affect the contact angle value measured to be 42°±3°in both situations.

Immobilizing the graphene with lipids is essential for contact angle measurement. If graphene is not stabilized with lipids, the action of placing the air bubble creates a momentum and pushes the graphene sheet away from the field of view of the camera, despite the fact that the bubble is stable and does not collapse.

For contact angle measurements of hydrogenated and oxygenated graphene, graphene was first hydrogenated (respectively, oxygenated) using a H_2 (respectively, O_2) plasma in a computer controlled Diener plasma generator for 247 seconds (1 mbar, 10 W).[10]

3.1.3. Raman spectroscopy

The quality and the number of layers of all graphene samples were characterized by Raman spectroscopy[11] at room temperature using a 100× objective and 457 nm and 532 nm lasers at a power below 2mW to avoid excessive thermal damage of graphene. Figure A3.3 of this Appendix displays typical Raman spectra of graphene on copper (Figure A3.3 a) and transferred onto a SiO_2/Si wafer (Figure A3.3 b). The shape of the 2D peak (~2700 cm^{-1}), that can be fitted with a single Lorenzian component is indicative of single-layer graphene.[11] The absence of a D peak at ~1370 cm^{-1} (Figure A3.3 a,b) suggests a low density of defects for non-treated graphene samples.[11]

For hydrogenated and oxygenated graphene, however, the appearance of the D peak (Figure A3.3 c,d) results from the introduced sp^3 defect sites.[10] Particularly, the ratio *I*(2D)//*I*(G) decreased from ~2 (pristine graphene) to ~1 after 4 min of hydrogen plasma treatment, indicating the effective doping in the lattice induced by hydrogenation.[12] Moreover, the appearance of a D' peak (~1620 cm^{-1}) in hydrogenated graphene is also related to the activation of defects. The *I*(D)/I(D') value of ~10 further confirms the sp^3 nature of hydrogenated defects.[13]

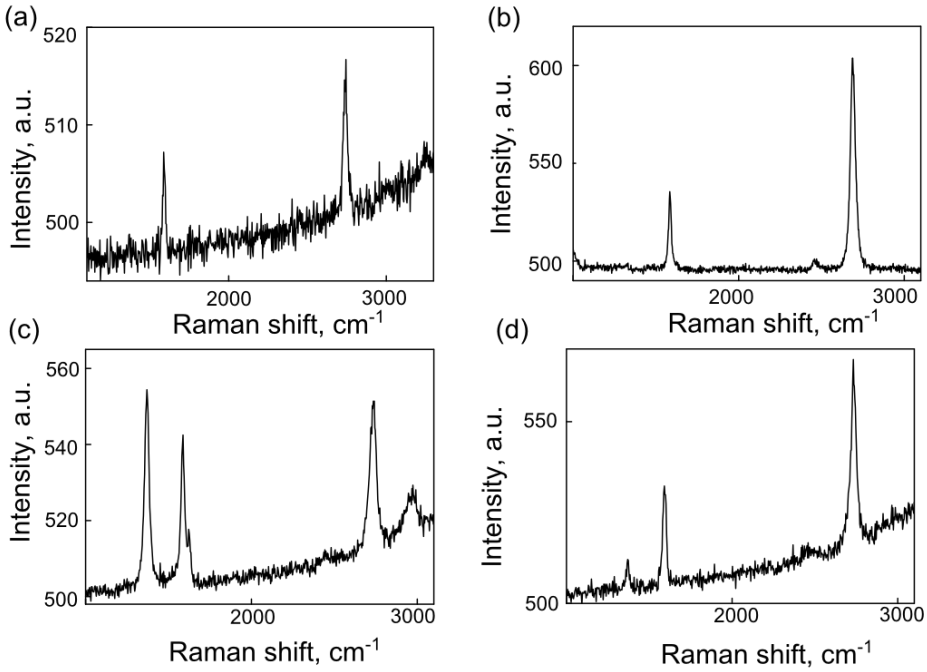

Figure A3.3. Raman spectra of CVD (chemical vapor deposition) graphene before and after plasma modification. (a) Non-treated graphene on Cu after the growth. (b) Non-treated graphene transferred onto a Si/SiO_2 wafer. (c) Graphene on Cu after H_2 plasma treatment. (d) Graphene on Cu after O_2 plasma treatment.

3.1.4. Optical microscopy

Optical images of graphene on water (Figure A3.4) and graphene transferred on silicon wafer were taken with a Leica optical microscope (DM 2700 M).

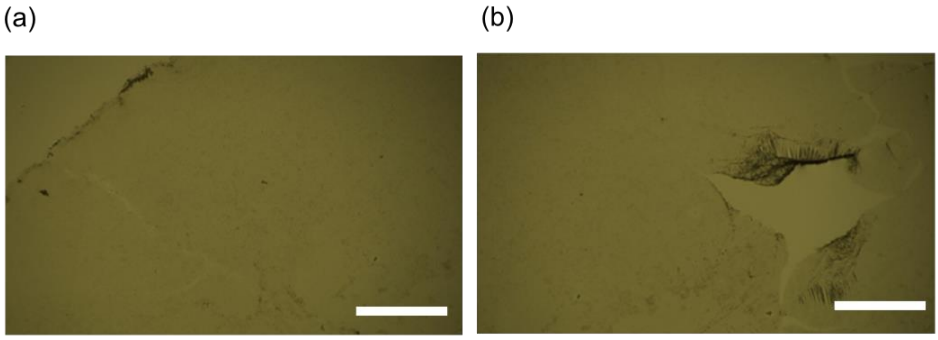

Figure A3.4. Optical images of graphene floating on the surface of water. (a) Before captive bubble measurement. The scale bar represents 500 µm. (b) After captive bubble measurement. The scale bar represents 500 µm.

3.1.5. Contact angle measurements

Contact angle measurements were conducted with a standard Ramé-Hart 250 goniometer (Netcong, NJ) and recorded with the DROPimage advanced v 2.8 software under ambient conditions (22°C). Two methods were used for the characterization of wetting. For the sessile drop technique a water droplet of 5-7 µL was deposited on a substrate and contact angle was measured within five seconds. For the captive bubble method, an air bubble with a volume of 6 µL was supplied with a microsyringe at the interface with an inverted needle (28 gauge, 304 SS Ramé-Hart). The analysis of contact angles from recorded videos were made with the software ImageJ (Drop snake analysis).

3.1.6. Measurements at different humidities

Experiments with controlled humidities were carried out using the saturated salt solution method, commonly used for accurate humidity control and the calibration of hygrometers.[57–59] For that, an oversaturated salt solution is placed in a closed box and certain equilibrium vapor pressure (and thus relative humidity) is created. The oversaturation of the solution assures that the built vapor pressure is stable to presence of moisture sources and sinks (the excess of the salt precipitates and the solution remains saturated with the vapor pressure

unchanged) and, therefore, provides a precise humidity level. Different salts have different saturated vapor pressures at a given temperature, and the humidity thus can be varied by changing the chemical composition of the salt.

For the experiments oversaturated solutions of KCl for the humidity of 85.11±0.29%[15] and K_2SO_4 for the humidity of 97.59±0.53% were used.[15] For measurements at every given humidity a beaker with the corresponding salt solution was placed in a sealed glass chamber with an embedded syringe (for further contact angle measurements) together with the cuvette containing graphene floating on water. Then the contact angle was measured using the captive bubble method. The relative humidity of 50% was the standard ambient humidity of the laboratory maintained by a moisture extractor and measured by a hygrometer, and the contact angle measurements were conducted without salt solutions.

3.2. Surface energy calculation

The surface energy and its components were calculated from the contact angle measurement of different liquids on target surfaces using the Owens-Wendt technique.[18] Ultrapure water, ethanol, ethylene glycol, diiodomethane, methylnaphthalene were used as test liquids.

Surface energies of bare PMMA (poly(methyl methacrylate) and PMMA-coated graphene samples were calculated according the Owens-Wendt model.[19] Based on the contact angle measurements with liquids of different polarities, the Owens-Wendt equation allows for the determination of total surface energy of a solid and its polar and dispersive components:

$$\gamma_{\mathrm{lv}}(1+\cos\theta) = 2\left(\sqrt{\gamma_{\mathrm{s}}^{\mathrm{d}}\gamma_{\mathrm{l}}^{\mathrm{d}}} + \sqrt{\gamma_{\mathrm{s}}^{\mathrm{p}}\gamma_{\mathrm{l}}^{\mathrm{p}}}\right)$$

The polar and dispersive components of liquids $\gamma_{\mathrm{L}}^{\mathrm{P}}$ and $\gamma_{\mathrm{L}}^{\mathrm{D}}$ were determined by measuring contact angles (sessile drop method) and applying the Owens/Wendt Theory for PTFE (teflon), which is a solid with known polar and dispersive

components of the surface tension (γ_S^P=0 mN m^{-1}, γ_S^D=18 mN m^{-1}). The determined surface tensions and their components of all used liquids are listed in Table A3.1.

Then contact angles of bare and PMMA-coated graphene with the liquids listed in Table A3.1 were measured. The results were plotted as $\frac{\gamma_L(cos\theta+1)}{2\sqrt{\gamma_L^D}}$ versus $\frac{\sqrt{\gamma_L^P}}{\sqrt{\gamma_L^D}}$ for each substrate and the dependences were fitted linearly. The slope of the plot equals $\sqrt{\gamma_S^P}$ and the intercept equals $\sqrt{\gamma_S^D}$. The squares of the latter two equal γ_S^P and γ_S^D respectively. The resulting surface tensions and their polar and dispersive components are presented in Table A3.2 below and charted in Figure 4.1c of Chapter 4.

Table A3.1. Calculated surface tensions, polar and dispersive components of tested liquids

Liquid	γ_L^P, mJ m^{-2}	γ_L^D, mJ m^{-2}	γ_L^{total}, mJ m^{-2}
Water	51	21.8	72.8 ± 2.4
Ethylene glycol	19.2	28.8	48.0 ± 1.9
10% Ethanol in water	36.1	23.9	60.0 ± 2.2
Diiodomethane	0	50.8	50.8 ± 2.3
1-Methylnaphthalene	0	42.0	42.0 ± 1.1

Table A3.2. Calculated surface tensions, polar and dispersive components of PMMA, freshly PMMA-coated graphene and PMMA-coated graphene aged for six days

Surface energy/Sample	PMMA	Graphene on PMMA	Graphene on PMMA after 6 days
γ_S^P, mN m^{-1}	9.8±1.6	10.8±1.5	9.1±1.4
γ_S^D, mN m^{-1}	41.9±1.3	39.1±2.1	30.6±2.4
γ_D^{total}, mN m^{-1}	51.6±2.3	47.9±1.6	39.7±1.5

3.3. References

1. Belyaeva, L. A., Fu, W., Arjmandi-Tash, H. & Schneider, G. F. Molecular caging of graphene with cyclohexane: transfer and electrical transport. *ACS Cent. Sci.* **2,** 904–909 (2016).

2. Suk, J. W. *et al.* Transfer of CVD-grown monolayer graphene onto arbitrary substrates. *ACS Nano* **5,** 6916–6924 (2011).

3. Batrakov, K. *et al.* Flexible transparent graphene/polymer multilayers for efficient electromagnetic field absorption. *Sci. Rep.* **4,** 7191 (2014).

4. Wu, B. *et al.* Experimental demonstration of a transparent graphene millimetre wave absorber with 28% fractional bandwidth at 140 GHz. *Sci. Rep.* **4,** 1–7 (2014).

5. Weissenborn P.K., Pugh, R. J. Surface tension of aqueous solutions of electrolytes: relationship with ion hydration, oxygen solubility, and bubble coalescence. *J. Colloid Interface Sci.* **184,** 550–563 (1996).

6. Hård, S. & Johansson, K. The surface tension of concentrated aqueous solutions of 1.1-electrolytes measured by means of Wilhelmy and laser light scattering methods. *J. Colloid Interface Sci.* **60,** 467–472 (1977).

7. Dutcher, C. S., Wexler, A. S. & Clegg, S. L. Surface tensions of inorganic multicomponent aqueous electrolyte solutions and melts. *J. Phys. Chem. A* **114,** 12216–12230 (2010).

8. Lima, L. M. C., Fu, W., Jiang, L., Kros, A. & Schneider, G. F. Graphene-stabilized lipid monolayer heterostructures: a novel biomembrane superstructure. *Nanoscale* **8,** 18646–18653 (2016).

9. Lima, L. M. C., Arjmandi-Tash, H. & Schneider, G. F. Lateral non-covalent clamping of graphene at the edges using a lipid scaffold. *ACS Appl. Mater. Interfaces* **10,** 11328–11332 (2018).

10. Jiang, L., Fu, W., Birdja, Y. Y., Koper, M. T. M. & Schneider, G. F. Quantum and electrochemical interplays in hydrogenated graphene. *Nat. Commun.* **9,** 793 (2018).

11. Ferrari, A. C. Raman spectroscopy of graphene and graphite: Disorder, electron-phonon coupling, doping and nonadiabatic effects. *Solid State Commun.* **143,** 47–57 (2007).

12. Das, A. *et al.* Monitoring dopants by Raman scattering in an electrochemically top-gated graphene transistor. *Nat. Nanotechnol.* **3,** 210–215 (2008).

13. Eckmann, A. *et al.* Probing the nature of defects in graphene by Raman spectroscopy. *Nano Lett.* **12,** 3925–3930 (2012).

14. Wexler, A., Brombacher, W. G. Methods of measuring humididty and testing hydrometers. *Ntational Bur. Stand.* **512,** 1–18 (1951).

15. Greenspan, L. Humidity fixed points of binary saturated aqueous solutions. *J. Res. Natl. Bur. Stand. Sect. A Phys. Chem.* **81A,** 89 (1977).

16. Lu, T. & Chen, C. Uncertainty evaluation of humidity sensors calibrated by saturated salt solutions. *Meas. J. Int. Meas. Confed.* **40,** 591–599 (2007).

17. Carotenuto, A. & Dell'Isola, M. An experimental verification of saturated salt solution-based humidity fixed points. *Int. J. Thermophys.* **17,** 1423–1439 (1996).

18. Kaelble, D. H. Dispersion-polar surface tension properties of organic solids. *J. Adhes.* **2,** 66–81 (1970).

19. Owens, D. K. & Wendt, R. C. Estimation of the surface free energy of polymers. *J. Appl. Polym. Sci.* **13,** 1741–1747 (1969).

APPENDIX 4

Supporting Information to Chapter 5

4.1. Methods

4.1.1. Graphene synthesis and transfer

Two types of CVD graphene were used: commercially purchased from Graphenea and synthesized in a cold-wall CVD oven.[1,2] For the latter, a copper foil with a thickness of 25 μm was annealed at 1035°C and the monolayer graphene films were grown according to the protocol described in ref.[3]. After the CVD synthesis, the graphene grown on the backside of the copper foil was removed by using oxygen plasma. Multilayer samples were purchased from Graphenea, where they were fabricated by the "repeat transfer" of monolayer graphene sheets on top of each other.

After etching the graphene on the backside of the copper foil, graphene samples were transferred to ice, hydrogel, PDMS and SiO_2/Si.

Graphene-on-ice. Copper with graphene on top was etched in an aqueous solution of 0.5 M ammonium persulfate (APS). After complete etching of the copper, the solution was placed at -20°C until the liquid was completely solidified. For several samples we replaced the etchant solution with pure water after the etching, with no effects on resulting contact angles (Figure A4.1 of this Appendix).

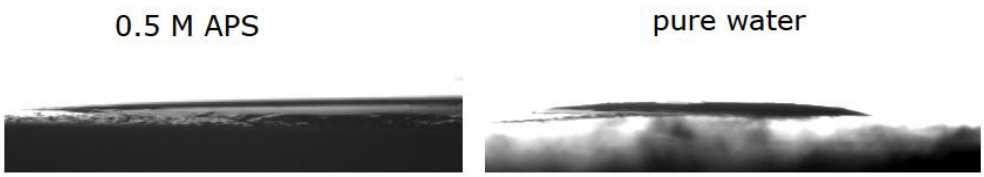

Figure A4.1. Water contact angle on frozen 0.5 M water solution of ammonium persulfate (APS) and pure water ice

Graphene-on-hydrogel. To ensure that the agarose-water ratio at this surface was the same as the bulk agarose-water ratio, a polystyrene petri dish was exposed to oxygen plasma for one minute to render the surface hydrophilic. A 4% agarose gel in deionized water was poured into the petri dish and then cut to 1 cm^3 cubes. With the side that had set against the hydrophilic glass surface facing up, the cubes were submerged halfway in 0.5 M APS, with a graphene/copper sample placed on top. Etching began when the APS solution diffused through the

gel matrix to the surface of copper. Typically complete copper etching occurred after 12 to 18 hours, resulting in a graphene layer 'floating' on top of the hydrogel. The sample was then soaked in pure water in order to replace the solution of ammonium persulfate and copper (II) ions with pure water. The integrity of graphene after this long etching time was confirmed by Raman spectroscopy.

Graphene on PDMS. A mixture of a silicone elastomer base and a silicone elastomer curing agent (Sylgard® 184, weight ratio 10:1) was prepared and left in the fridge for 1.5 hours for degassing. Then a graphene/copper piece was placed onto PDMS with the copper side facing upwards. After that, PDMS was cured in an oven at 80°C for one hour. When PDMS was solidified the PDMS/graphene/copper stack was placed on the surface of 0.5 M water solution of ammonium persulfate for etching the copper. After copper was etched graphene was rinsed with water to wash away the ammonium persulfate salt crystals. Then the contact angle was measured. Before preparing graphene-on-PDMS sample, graphene on copper was annealed and then placed onto PDMS with the copper side facing upwards, such that hydrocarbons adsorption was avoided for these samples. Thus, graphene was only exposed to air for a time period not longer than 5 minutes. The surface morphology of graphene on PDMS was inspected using AFM (Figure A4.2 of this Appendix).

Graphene on SiO_2/Si. To transfer graphene onto a SiO_2/Si wafer we used the conventional PMMA-assisted method reported in ref.[4]. Prior to the transfer, wafers were cleaned in several steps following a procedure similar to described in ref.[5–7] The wafers were first cleaned with cotton swap soaked with ethanol to remove big particles. Thereafter, the wafers were rinsed with water, acetone, isopropanol and ethanol and blow-dried with argon. Then the wafers were immersed in a piranha solution for 5 minutes (1 part H_2O_2 and 3 parts H_2SO_4) to remove residues of the organic solvents and, finally, rinsed with ultrapure water. The surface morphology of graphene on SiO_2/Si was inspected using AFM (Figure A4.2 of this Appendix).

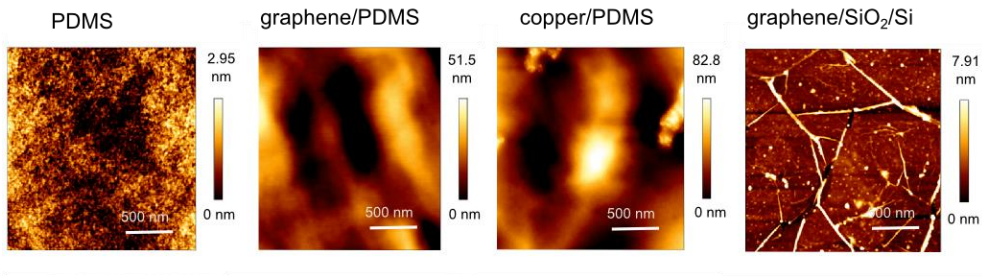

Figure A4.2. Surface morphology of PDMS and SiO_2/Si graphene substrates imaged by AFM. The high corrugation of graphene on PDMS compared to bare PDMS stems from the copper foil on which graphene was grown and brought into contact with PDMS before it was cured. For PDMS deposited on bare copper (no graphene present) and graphene on PDMS similar roughness is seen. The contact angle on the graphene-on-PDMS surface may be influenced by the corrugation and no longer governed by wetting transparency. Graphene deposition on SiO_2/Si involves polymer transfer, and typically results in wrinkled graphene and even polymer residues, resulting in poorer conformity and irreproducible contact angles

4.1.2. Contact angle measurements

Contact angle measurements are very sensitive to any contamination of the surface, therefore, great care should be taken in order to keep the samples as clean as possible. Liquids that were used for contact angle measurements are listed in Table A4.1 of this Appendix.

Table A4.1. Solvents for contact angle measurements

Test liquid	$\sigma_{L,}$ mN/m	σ_L^D, mN/m	σ_L^P, mN/m	Freezing point,°C	Substrates
water	72.8	26.4	46.4	0	Ice, hydrogel, SiO_2/Si, PDMS, copper
diiodomethane	50.8	44.4 to 50.8	0	5.4 to 6.2	Hydrogel, SiO_2/Si, PDMS, copper
1-methylnaphtalene	30.06-38.7	20.6	0.8	-22	Hydrogel
methylbenzoate	37.2	27	10.2	-12.5	Ice, SiO_2/Si, PDMS, copper
nitromethane	36.5	22	14.5	-29	Ice, SiO_2/Si, PDMS, copper
ethylene glycol	47.7	26.4	21.3	-12.9	Ice, SiO_2/Si, PDMS, copper
formamide	57	39	19	2 to 3	SiO_2/Si, PDMS, copper

Graphene-on-ice

Contact angle (CA) measurements with ice were performed at 0°C (with pure water) and -20°C (water with addition of nitric acid). Although experiments with ice are fairly straightforward, one should account for several technical difficulties accompanying measurements at temperatures below 0°, namely condensation and freezing of the droplet. We minimized the effect of condensation by constantly flushing the chamber with dry air. Control experiments with graphite and a Si/SiO_2 wafer confirmed no effect of condensation on the water contact angle (see Figure A4.3 of this Appendix). Control experiments with graphite at temperatures below 0°C showed that the addition of nitric acid has negligible effects on the contact angle. Contact angles with pure water and 18% nitric acid

are equal within the margins of experimental error (see Figure 5.2a of Chapter 5).

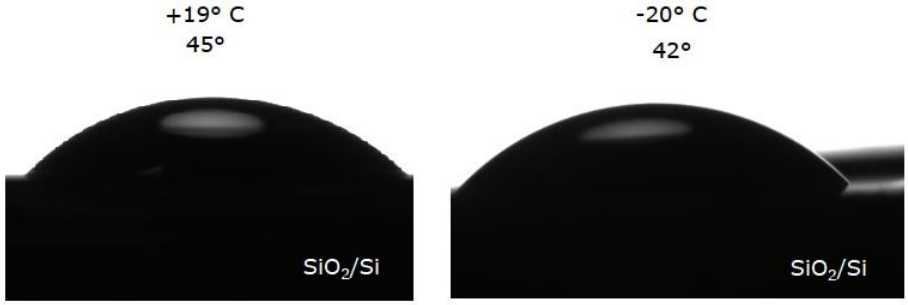

Figure A4.3. Control water contact angle on SiO_2/Si under ambient conditions (left) and under conditions identical to the measurements with ice (right). For the latter the wafer was placed on the surface of water solution of ammonium persulfate and then cooled down to -20°C in Peltier chamber with constant flushing the chamber with dry air. No significant difference in WCA was detected

Raman characterization was not possible for graphene on ice. Ice starts melting as soon as the laser hits the graphene surface, and even when kept in cold. Additionally, the signal from ice appears to be much more intensive not allowing to detect any of the graphene typical bands. A typical Raman spectrum of graphene on ice is presented in Figure A4.4 of this Appendix.

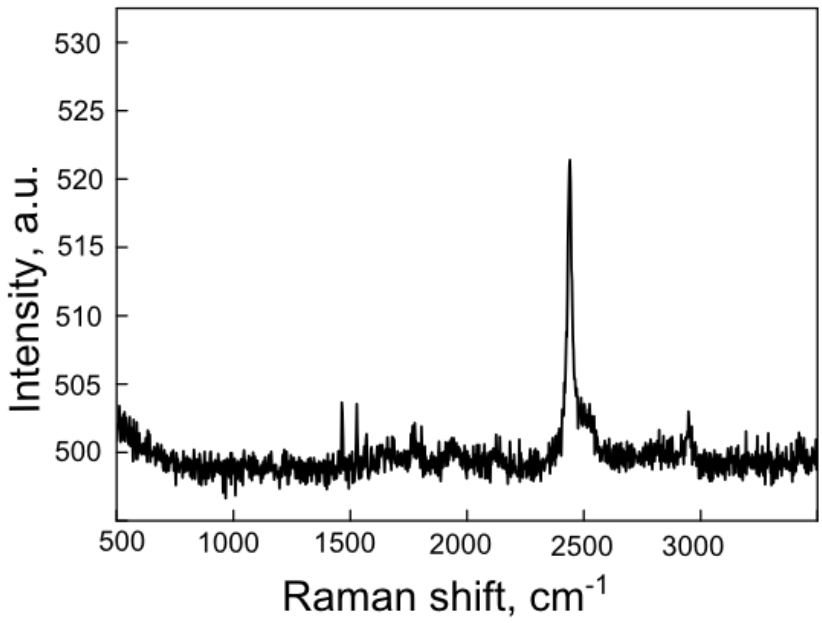

Figure A4.4. Typical Raman spectrum of graphene on ice (laser wavelength 532 nm): no graphene bands are detectable.

For ice we cannot completely avoid exposure to ambient air, those samples are normally exposed air for 1-1.5 hour. For that reason, experiments in controlled atmosphere were performed on graphene that had been minimally exposed to ambient atmosphere. Graphene on copper was thermally annealed and then directly transferred into the controlled N_2 atmosphere of a glove bag (Aldrich® Atmosbag), where etching was performed. The sample was then cooled down at -20°C. Contact angles were then taken in ambient atmosphere within 5 min and did not show any measurable difference between the samples measured in ambient and controlled atmospheres (Figure A4.5 of this Appendix).

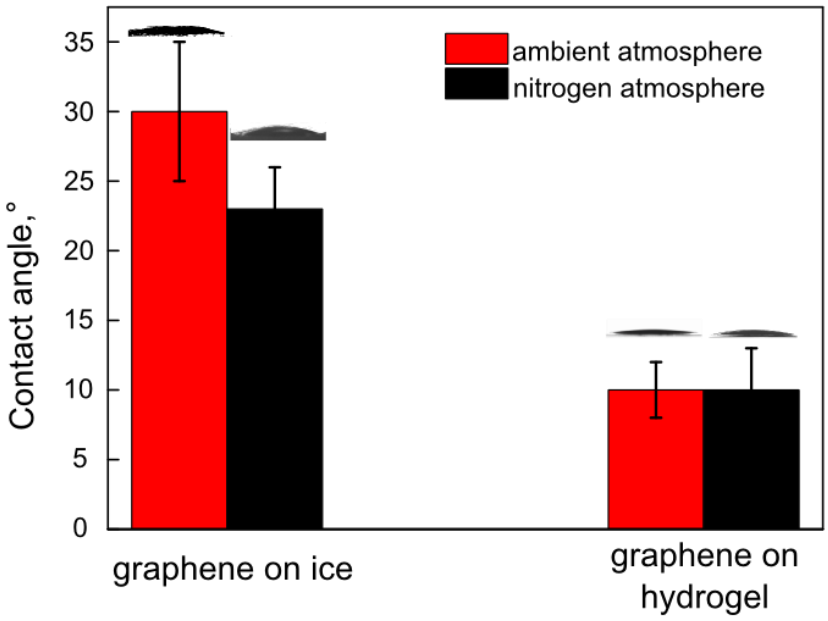

Figure A4.5. Water contact angles of graphene on ice and graphene on hydrogel prepared in ambient atmosphere (red) and controlled atmosphere of nitrogen (black)

Graphene-on-hydrogel

A 4% agarose (w/w) was used to support CVD grown graphene from the beginning of the etching process until CA is measured. To confirm that during the contact angle measurements the hydrogel matrix did not contain any impurities and/or residuals from the etching process of copper, Atomic Force Microscopy (AFM) and Raman spectroscopy were performed on graphene-on-hydrogel (Figure A4.6 of this Appendix).

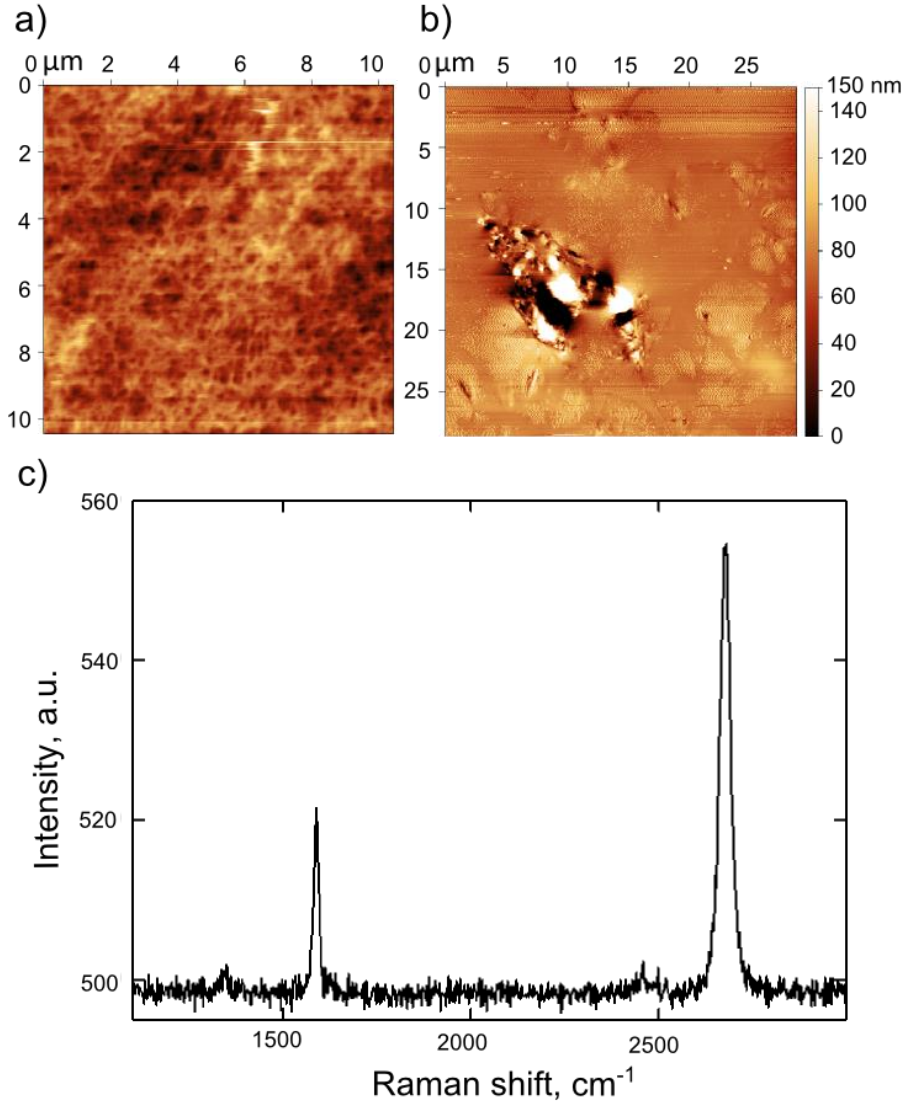

Figure A4.6. Characterization of graphene on hydrogel. a) AFM image of bare hydrogel. b) AFM image of graphene on hydrogel. c) Raman spectrum of graphene on hydrogel.

For hydrogel we cannot completely avoid exposure to ambient air, those samples are normally exposed air for 13-18 hours. For that reason, experiments in

controlled atmosphere were performed on graphene that had been minimally exposed to ambient. Graphene on copper was thermally annealed and directly transferred into the controlled N_2 atmosphere of a glove bag (Aldrich® Atmosbag), where etching on hydrogel was performed. Contact angles were then taken in ambient atmosphere. The total time that the graphene surface was exposed to ambient conditions before contact angle measurement never exceeded 5 minutes (Figure A4.5 of this Appendix). These control experiments did not show any measurable difference between the samples measured in ambient and controlled atmospheres (Figure A4.5 of this Appendix).

In addition to the linear extrapolation for diiodomethane (Figure 5.2c of Chapter 5), the linear extrapolation of the CA of 1-methylnaphtalene on hydrogel based on agarose concentration of 1 to 4% agarose was also made, showing that the CA of 1-methylnaphtalene on water would be 25° (Figure A4.7 of this Appendix).

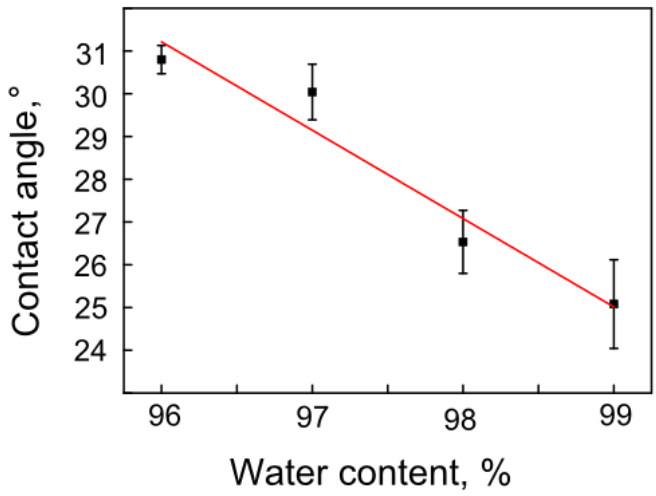

Figure A4.7. Hydrogel as a water model: contact angle of 1-methylnaphtalene on an agarose hydrogel with different water content

Graphene on copper, SiO_2/Si and PDMS

Graphene on copper, SiO_2/Si and PDMS were prepared as described in the above section. The transferred samples were then annealed at 550°C for one hour

under 100 mbar. Contact angle measurements were conducted within 3 min after the annealing. In general, no difference in contact angle was detected for samples probed right after the annealing and 48 hours later (see Figure A4.8 of this Appendix).

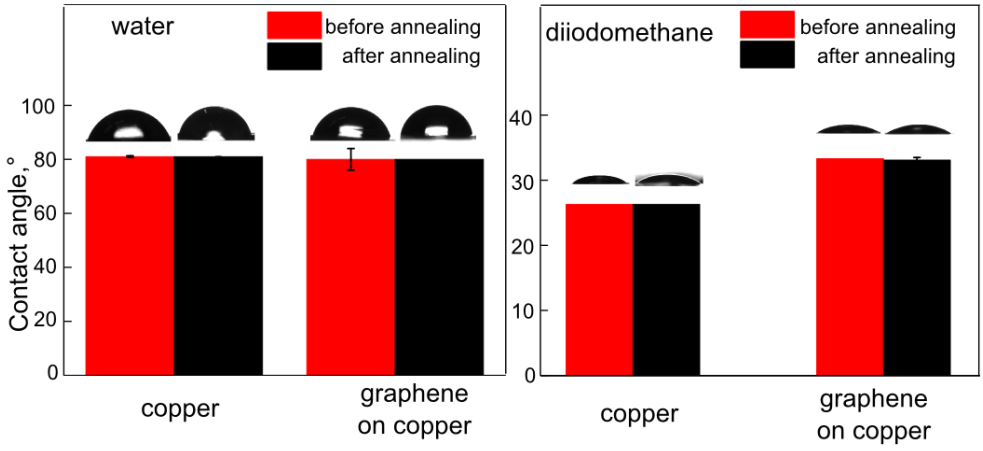

Figure A4.8. Contact angles of copper and graphene on copper with water and diiodomethane before and after annealing.

Contact angles of mono-, bi-, tri- and four-layer graphene on copper with water and diiodomethane did not show measurable difference (Figure A4.9 of this Appendix).

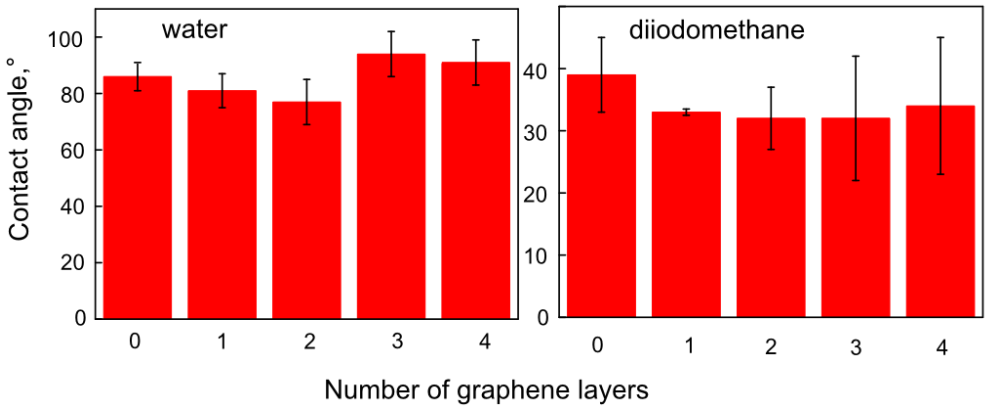

Figure A4.9. CA of water and diiodomethane on mono-, bi-, three- and four-layer graphene on copper.

Samples of graphene transferred to SiO_2/Si substrates showed high sample-to-sample variations and irreproducible contact angle values (Figure A4.10 of this Appendix).

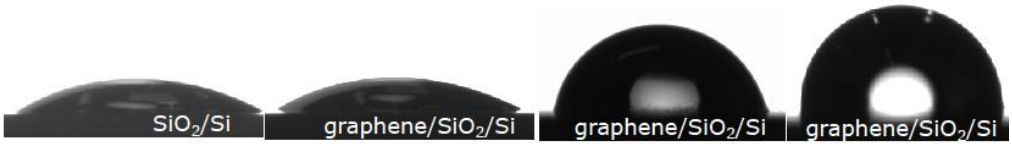

Figure A4.10. Irreproducibility of the WCA of graphene transferred onto SiO_2/Si wafers: WCA of bare SiO_2/Si wafer and WCA of graphene transferred onto SiO_2/Si wafer for different samples.

PDMS samples underwent exactly the same treatment steps as graphene/PDMS samples: after curing, PDMS was incubated in the APS solution for one hour, then rinsed with water and then the contact angle was measured.

4.2. Calculation of polar and dispersive components by Owens-Wendt method

Contact angles of all samples with the liquids listed in Table A4.1 of this Appendix were measured. Then the results were plotted as $\frac{\sigma_L(cos\theta+1)}{2\sqrt{\sigma_L^D}}$ versus $\frac{\sqrt{\sigma_L^P}}{\sqrt{\sigma_L^D}}$ (see Figure A4.11 of this Appendix) for each substrate and the dependences were fitted linearly. The slope of the plot equals $\sqrt{\sigma_S^P}$ and the intercept equals $\sqrt{\sigma_S^D}$. The square of the latter two equals σ_S^P and σ_S^D respectively.

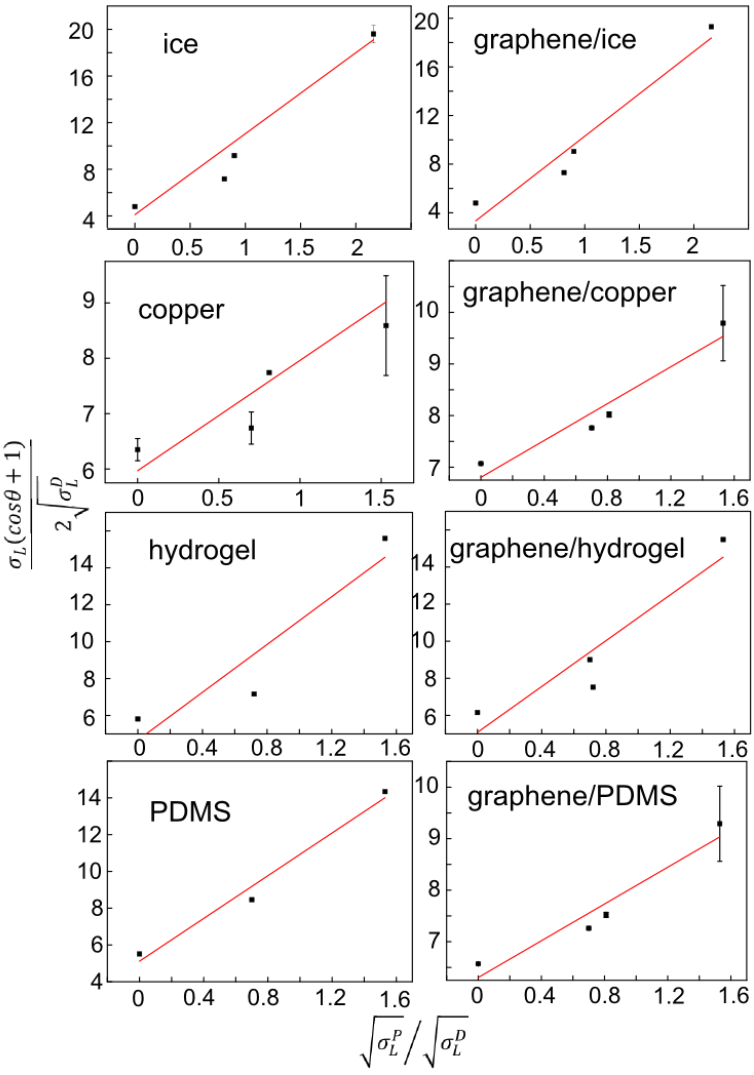
ice
graphene/ice
copper
graphene/copper
hydrogel
graphene/hydrogel
PDMS
graphene/PDMS
$\frac{\sigma_L(cos\theta+1)}{2\sqrt{\sigma_L^D}}$
$\sqrt{\sigma_L^P}/\sqrt{\sigma_L^D}$

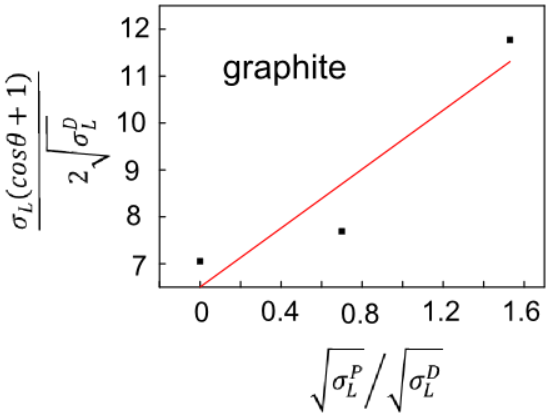

Figure A4.11. Owens-Wendt plots for ice, graphene/ice, copper, graphene/copper, hydrogel, graphene/hydrogel, PDMS, graphene/PDMS and graphite.

4.2.1. Calculation of the polar and dispersive components for 18% HNO_3

To determine the polar and dispersive components of 18% HNO_3 we applied the Owens/Wendt Theory for teflon, which is a solid with known polar and dispersive components of the surface tension (σ_S^P=0mN/m, σ_S^D=18 mN/m). CA between the teflon plate and nitric acid solution was found to be 96.8°±0.2. The total surface tension of 18% HNO_3 was calculated according the model described in ref.[8] and is equal to 69.26 mN/m.

In this way the Owens/Wendt equation reduces to $\sigma_L^D = \frac{(\sigma_L\ (cos\theta+1))^2}{72}$= 57 mN/m and $\sigma_L^P = \sigma_L\ - \sigma_L^D$=12.26 mN/m.

4.2.2. Comparison with the Fowkes method

Surface energies calculated by Owens-Wendt and Fowkes methods agree within experimental error margins (Figure A4.12 of this Appendix).

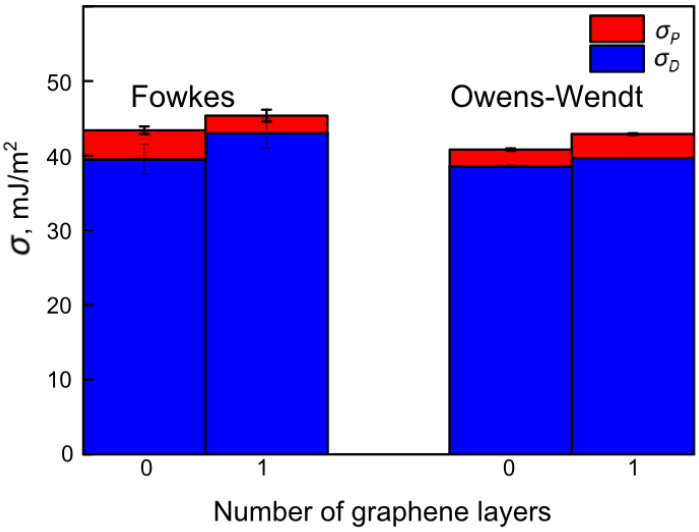

Figure A4.12. Polar and dispersive components of the surface tensions of bare copper and graphene/copper calculated by Fowkes and Owens-Wendt models.

4.3. References

1. Pierson, H. O. *Handbook of chemical vapor deposition (CVD)*. (Noyes Publications / William Andrew Publishing, LLC, 1999).

2. Muñoz, R. & Gómez-Aleixandre, C. Review of CVD synthesis of graphene. *Chem. Vap. Depos.* **19,** 297–322 (2013).

3. Arjmandi-Tash, H., Lebedev, N., van Deursen, P., Aarts, J. & Schneider, G. F. Hybrid cold and hot-wall chamber for fast synthesis of uniform graphene. *Carbon N. Y.* **118,** 438–442 (2017).

4. Suk, J. W. *et al.* Transfer of CVD-grown monolayer graphene onto arbitrary substrates. *ACS Nano* **5,** 6916–6924 (2011).

5. Wang, Q. H. *et al.* Understanding and controlling the substrate effect on graphene electron-transfer chemistry via reactivity imprint lithography. *Nat. Chem.* **4,** 724–732 (2012).

6. Shim, J., Rivera, J. A. & Bashir, R. Electron beam induced local crystallization of HfO_2 nanopores for biosensing applications. *Nanoscale* **5,** 10887–93 (2013).

7. Kim, S. S. *et al.* Strain-assisted wafer-scale nanoperforation of single-layer graphene by arrayed Pt nanoparticles. *Chem. Mater.* **27,** 7003–7010 (2015).

8. Dutcher, C. S., Wexler, A. S. & Clegg, S. L. Surface tensions of inorganic multicomponent aqueous electrolyte solutions and melts. *J. Phys. Chem. A* **114,** 12216–12230 (2010).

APPENDIX 5

Supporting Information to Chapter 6

5.1. Methods

5.1.1. Sample preparation

All graphene samples were grown using the same CVD protocol.[1] The as-grown samples were grown directly on Cu(111) and on polycrystaline copper substrates that were further studied in TPD. The transferred graphene was first grown on copper foil and then transferred to a polycrystalline copper substrate using the PMMA-assisted transfer method.[2] All samples were characterized with Raman spectroscopy at an excitation wavelength of 457 nm.

5.1.2. TPD measurements

TPD experiments were performed in a home-built UHV apparatus with a differentially pumped quadrupole mass spectrometer.[3] The procedure that corrects for the changing background pressure during a TPD experiment has also been described previously.[4] After introducing copper samples with transferred or as-grown graphene into the UHV chamber, the samples were annealed at modest temperatures (~400 K) to remove contaminants. Ultrahigh purity water was dosed from a capillary array doser onto the sample. After a series of water TPD spectra for various water coverages on graphene were obtained, graphene was removed by cycles of Ar^+ sputtering at 1 kV and annealing at ~900 K. From the cleaned Cu substrates, water desorption was also studied by the same procedures. All TPD spectra were obstained using a temperature ramp of ~1.0 K/s.

5.1.3. Contact angle measurements

To prevent copper oxydation upon exposure to air, bare copper crystals were annealled at 500°C in hydrogen atmosphere. The contact angles were measured right after (*i.e.* within 1-2 minutes) and 30 minutes after the annealing. When graphene is grown on copper substrate (which was pre-annealed), it protects the copper surface from oxidation, and, therefore, no copper oxide layer was formed in the samples of graphene grown on copper. However, to remove the adsorbed airborne hydrocarbons[5] all graphene samples were also annealed right before

contact angle measurements. Additional Raman spectra of the Cu samples were taken after removal of graphene by sputtering in UHV and re-exposing the samples to air.

5.2. References

1. Fu, W. *et al.* Graphene transistors are insensitive to pH changes in solution. *Nano Lett.* **11,** 3597–3600 (2011).

2. Suk, J. W. *et al.* Transfer of CVD-grown monolayer graphene onto arbitrary substrates. *ACS Nano* **5,** 6916–6924 (2011).

3. Badan, C., Koper, M. T. M. & Juurlink, L. B. F. How well does Pt(211) represent Pt[n (111) × (100)] surfaces in adsorption/desorption? *J. Phys. Chem. C* **119,** 13551–13560 (2015).

4. den Dunnen, A., van der Niet, M. J. T. C., Koper, M. T. M. & Juurlink, L. B. F. Interaction between H_2O and preadsorbed D on the stepped Pt(553) surface. *J. Phys. Chem. C* **116,** 18706–18712 (2012).

5. Li, Z. *et al.* Effect of airborne contaminants on the wettability of supported graphene and graphite. *Nat. Mater.* **12,** 925–931 (2013).